Structural Eng./Earthquake Eng., JSCE, Vol. 15, No. 2, 155s—163s, 1998 July
(J. Struct. Mech. Earthquake Eng., JSCE, No. 598/ I —44)

A TRANSIENT RESPONSE ANALYSIS OF A VERY LARGE FLOATING STRUCTURE BY FINITE ELEMENT METHOD

Eiichi WATANABE[1], Tomoaki UTSUNOMIYA[2]and Shinkichi TANIGAKI[3]

[1]Fellow of JSCE, Ph.D., Dr.Eng., Professor, Dept. of Civil Engineering, Kyoto University (Sakyo-ku, Kyoto 606-01, Japan)
[2]Member of JSCE, Dr.Eng., Associate Professor, Dept. of Civil Engineering, Kyoto University (Sakyo-ku, Kyoto 606-01, Japan)
[3]Member of JSCE, M.S., Technical Headquarters, Mitsubishi Heavy Industries, Ltd. (Nagasaki 851, Japan)

Presented herein is a transient response analysis of a VLFS (Very Large Floating Structure) due to impulsive landing of an airplane by Finite Element Method. The wave absorption filter which consists of sponge layer and Sommerfeld boundary is applied to open boundaries with irregular waves, and has been found to be efficient. The dynamic deflectional configuration caused by the landing of an airplane appears to be axisymmetric with respect to the point of landing for a few seconds after the landing; however, after that, the response becomes non axisymmetric depending on the shape of the floating body.

Key Words : *VLFS, FEM, transient response, sponge filter, fluid-structure interaction*

1. INTRODUCTION

It is of great importance to investigate dynamic response pertaining to the serviceability and the safety of floating airport against the waves, winds, and the landing load of airplanes. In case of small floating structures, the elastic response is smaller than the rigid body motion; in case of very large floating structures (VLFS), however, the depth is much smaller than the horizontal dimensions and thus the floating structures tend to be very flexible[1),2)]. Thus, questions arise if the effect is controllable on the safety facilities for the landing of airplanes in case a VLFS is used as an airport.

One of such questions may be directed toward the effect of the deflection of the deck plate due to the landing of an airplane on the guiding system called Precision Approach Path Indicator, PAPI, regarding the possibility of sending erroneous indications to the succeeding airplane in the air, waiting for landing. The PAPI is a unit of indicator lights on either side of runway installed near the edge of the runway. As an aircraft approaches, the indicator lights change to either white or red to convey to the pilot the error in the angle of approach path[2)]. This concern may be so important as to be necessarily answered for the implementation of floating airport.

Two of the present authors have already presented a transient response analysis of axisymmetric floating plate with closed fluid domain by Finite Element Method (F.E.M.)[3),4)]. In the analysis with the closed fluid domain, the radiation waves generated by the plate vibration are reflected at the boundary wall; thus large distance between the boundary wall and the structure is required in order to obtain an equivalent solution for open sea. Therefore, when the same method is applied to a general 3-dimensional analysis, requirement of large storage limits the size of the structure. Therefore, in order to analyze a large structure such as a floating airport, open boundary condition should be satisfied at the finite (and desirably small) distance from the structure, which will reduce the size of F.E.M. model.

In case of a single wave frequency, the analysis could be extended to non-reflecting open boundaries by use of the Sommerfeld boundary condition. However, in such a transient problem as the airplane landing, many frequencies will be included in the radiation waves, and thus the Sommerfeld condition alone is insufficient to disperse the wave energy and another appropriate method for unbounded boundary is required.

The main purpose of this study is to analyze the dynamic deflectional response of a very large

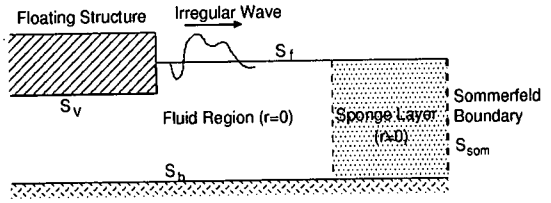

Fig. 1 Numerical wave absorption filter

floating structure at the airplane landing in the time domain. Considered herein in particular is the application of an wave absorption filter which consists of sponge layer and Sommerfeld boundary developed by Ohyama and Nadaoka[5]. The finite element method is adopted for the axisymmetric problem at first, with an open boundary problem. Then, an attempt is made to extend it to the 3-dimensional problem and the time domain analysis is performed by simplifying the landing load of a Jumbo jet plane.

2. METHOD OF ANALYSIS

(1) Wave Absorption Filter

The Sommerfeld boundary has been used almost exclusively for the absorption of waves beyond certain domain. However, it assumes a single wave velocity and thus, for irregular waves, the wave energy is only insufficiently reduced. Instead of this type of boundary, an attempt is made using the numerical wave filter as shown in **Fig.1**[5]. This wave absorption filter consists of the sponge layer which is characterized by the damper to absorb the wave energy and a Sommerfeld boundary surrounding it. The wave absorption mechanism of the sponge filter is considered to be very effective even against the irregular waves since it is based on the energy absorption due to the friction of the passing fluid and does not have significant frequency dependence. Only one caution may be such that when the length of an incidental wave component happens to be larger than the radius of the sponge layer, then the energy absorption may not be sufficient. Thus, for this long wave length, the Sommerfeld boundary located outside of the sponge layer may work effectively to disperse the energy by taking into account the fact that the long wave velocity, c, can be approximated by velocity $\sqrt{gh}$ where g and h refers to the gravity and the depth of the fluid, respectively.

(2) Formulation by Finite Element

The equilibrium equation for small motions of a compressible and inviscid fluid flowing through a resisting matrix material can be written as follows:

$$\nabla p + r\dot{\mathbf{u}} + \rho\ddot{\mathbf{u}} = \mathbf{O} \tag{1}$$

$$p = -B\nabla \cdot \mathbf{u} \tag{2}$$

where p refers to the dynamic pressure; $\mathbf{u}$, $\dot{\mathbf{u}}$, and $\ddot{\mathbf{u}}$ the fluid particle displacement, velocity, and acceleration, respectively; ρ the density of the fluid; r the volumetric drag coefficient (force per unit volume per velocity); and B the bulk modulus of the fluid. In this study, constant value of r is applied at the sponge layer surrounding the fluid region. In the fluid region, no drag resistant is applied, i.e., $r = 0$.

Based on the linear wave theory, appropriate boundary conditions can be represented as follows:

$$\mathbf{n} \cdot \ddot{\mathbf{u}} = 0 \quad \text{on } S_b \tag{3}$$

$$\mathbf{n} \cdot \ddot{\mathbf{u}} = \mathbf{n} \cdot \ddot{\mathbf{u}}^m \quad \text{on } S_V \tag{4}$$

$$\mathbf{n} \cdot \dot{\mathbf{u}} = \frac{1}{\rho g}\dot{p} \quad \text{on } S_f \tag{5}$$

$$\mathbf{n} \cdot \dot{\mathbf{u}} = \frac{1}{\rho\sqrt{gh}}p \quad \text{on } S_{som} \tag{6}$$

where $\mathbf{n}$ represents the outward unit normal vector out of the fluid region at the boundaries, $\ddot{\mathbf{u}}^m$ represents the acceleration of the structural media at the fluid-structure boundary, and S_b, S_V, S_f and S_{som} are the boundaries on the sea bottom, on the wetted body surface, on the free surface and on the Sommerfeld boundary, respectively.

When $\nabla\cdot$ is applied to Eq. (1), the following equation is obtained:

$$\nabla \cdot \frac{1}{\rho}\nabla p + \nabla \cdot (\mu\dot{\mathbf{u}}) + \nabla \cdot \ddot{\mathbf{u}} = 0 \tag{7}$$

where

$$\mu = \frac{r}{\rho}. \tag{8}$$

If μ = constant in an element, then $\nabla \cdot \mu = 0$. Besides, substitution of Eq. (2) into Eq. (7) yields

$$\frac{1}{B}\ddot{p} + \frac{\mu}{B}\dot{p} - \nabla \cdot \frac{1}{\rho}\nabla p = 0 \tag{9}$$

Next, let us consider the integration of the weighted integrand of Eq. (9) with the weight, w:

$$\begin{aligned}
&\int_V w\left\{\frac{1}{B}\ddot{p} + \frac{\mu}{B}\dot{p} - \nabla \cdot \frac{1}{\rho}\nabla p\right\} dV \\
&= \int_V w\frac{1}{B}\ddot{p}\,dV + \int_V w\frac{\mu}{B}\dot{p}\,dV \\
&\quad + \int_V \nabla w \cdot \frac{1}{\rho}\nabla p\,dV - \int_S w\frac{1}{\rho}\nabla p \cdot d\mathbf{S} \\
&= 0
\end{aligned} \tag{10}$$

where $\mathbf{S}$ refers to the outward normal vector at the boundary, and $d\mathbf{S} = \mathbf{n}dS$.

For the formulation by Finite Element Method, the fluid and sponge parts should be divided into many regions considering the pressure, p, as unknown being designated in terms of the joint pressure vector, $\mathbf{p}$, and the shape function, $\mathbf{N}$, so that

$$p = \mathbf{N}^T\mathbf{p} \tag{11}$$

Moreover, adopting $\mathbf{N}$ for the weighting function, w, the following discretization can be made:

$$\begin{aligned}
&\int_V \mathbf{N}\frac{1}{B}\mathbf{N}^T\ddot{\mathbf{p}}\,dV + \int_V \mathbf{N}\frac{\mu}{B}\mathbf{N}^T\dot{\mathbf{p}}\,dV \\
&+ \int_V \nabla\mathbf{N}\cdot\frac{1}{\rho}\nabla\mathbf{N}^T\mathbf{p}\,dV - \int_S \mathbf{N}\frac{1}{\rho}\nabla p\cdot d\mathbf{S} \\
&= \int_V \mathbf{N}\frac{1}{B}\mathbf{N}^T\,dV\ddot{\mathbf{p}} + \int_V \mathbf{N}\frac{\mu}{B}\mathbf{N}^T\,dV\dot{\mathbf{p}} \\
&+ \int_V \nabla\mathbf{N}\cdot\frac{1}{\rho}\nabla\mathbf{N}^T\,dV\mathbf{p} - \int_S \mathbf{N}\frac{1}{\rho}\nabla p\cdot d\mathbf{S} \\
&= \mathbf{O}
\end{aligned} \tag{12}$$

where the first three terms of Eq. (12) designate the volume integrals of the interior of the element; the 4th term, on the other hand, designates the boundary integrals. Upon substitution of appropriate boundary conditions Eqs. (3)-(6) into Eq. (12) wherein $\nabla p = -r\dot{\mathbf{u}} - \rho\ddot{\mathbf{u}}$ (Eq. (1)) is utilized, the following equation can be obtained:

$$\begin{aligned}
&(\mathbf{M}+\mathbf{M}_f)\ddot{\mathbf{p}} + (\mathbf{C}+\mathbf{C}_f+\mathbf{C}_{som})\dot{\mathbf{p}} \\
&\quad +(\mathbf{K}+\mathbf{K}_{som})\mathbf{p} + \mathbf{M}_V\ddot{\mathbf{u}}^m = 0
\end{aligned} \tag{13}$$

where

$$\begin{aligned}
\mathbf{M} &= \int_V \mathbf{N}\frac{1}{B}\mathbf{N}^T\,dV \\
\mathbf{M}_f &= \int_{S_f} \mathbf{N}\frac{1}{\rho g}\mathbf{N}^T\,dS \\
\mathbf{C} &= \int_V \mathbf{N}\frac{\mu}{B}\mathbf{N}^T\,dV \\
\mathbf{C}_f &= \int_{S_f} \mathbf{N}\frac{\mu}{\rho g}\mathbf{N}^T\,dS \\
\mathbf{C}_{som} &= \int_{S_{som}} \mathbf{N}\frac{1}{\rho\sqrt{gh}}\mathbf{N}^T\,dS \\
\mathbf{K} &= \int_V \nabla\mathbf{N}\cdot\frac{1}{\rho}\nabla\mathbf{N}^T\,dV \\
\mathbf{K}_{som} &= \int_{S_{som}} \mathbf{N}\frac{\mu}{\rho\sqrt{gh}}\mathbf{N}^T\,dS \\
\mathbf{M}_V &= \int_{S_V} \mathbf{N}\mathbf{n}\cdot\mathbf{N}_m^T\,dS
\end{aligned}$$

where $\mathbf{M}$, $\mathbf{C}$, and $\mathbf{K}$ refer to the mass, damping and stiffness matrix, respectively. Wherever there are no suffices, they imply the interior of the fluid and the suffices f, V and som refer to the free surface, boundary between the fluid and the floating body and the Sommerfeld boundary, respectively. Moreover, $\ddot{\mathbf{u}}^m$ refers to the acceleration of the structure; $\mathbf{N}_m$ refers to the shape function of displacement of structures.

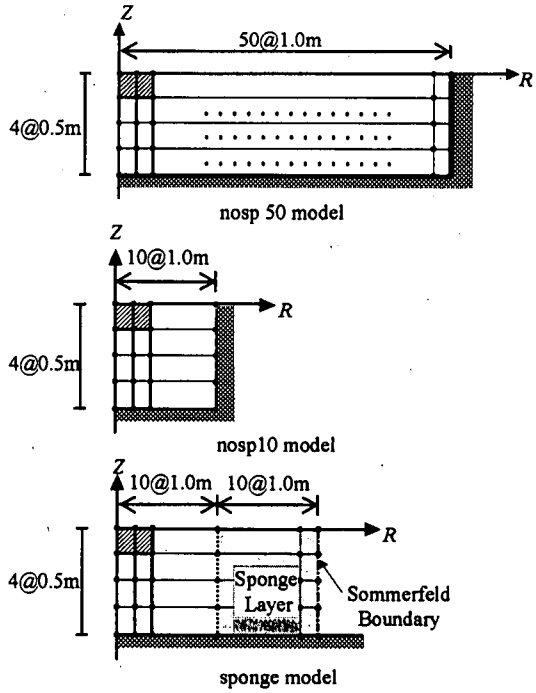

Fig. 2 Axi-symmetric sponge and non-sponge elements

The computation is performed by ABAQUS which is a general purpose finite element program. ABAQUS[7),8)] has some elements for acoustic analysis and their formulation is equivalent to Eq. (13), so that we have been able to apply such acoustic elements to the transient response analysis of a VLFS. In the transient analysis, Newmark-β method is applied with $\beta = 0.25$.

3. RESULTS OF ANALYSIS AND DISCUSSIONS

(1) Verification of Sponge Elements

At first, in axisymmetric problems, the applicability of the sponge elements will be studied. The model used is shown in **Fig.2**. In this figure, "nosp L" refers to non sponge elements but with the rigid wall placed at L m from the axis of axisymmetry; while "sponge" refers to the model with the sponge layer extending from 10 m from the axis over the length of 10 m and with the volumetric drag coefficient, r, and with a Sommerfeld boundary at the exterior boundary. The other features of the model are provided in **Table 1**.

Table 1 Characteristics of verification model

Young's Modulus	6.617×10^{11} kN/m^2
Density of Fluid	1.025 ton/m^3
Draft	0.5 m
Depth of Water	2 m

Now let us consider a floating structural model of radius 2 m to which a sinusoidal wave with the amplitude of 0.5 m is forced. The structural elements are 4-node linear hybrid nonconforming axisymmetric elements; while 4-node axisymmetric acoustic elements are used for the fluid domain, of which definitions are found in Eq. (13) as $\mathbf{M}$, $\mathbf{C}$ and $\mathbf{K}$, and 2-node axisymmetric elements are used for the boundaries, of which definitions are also found in Eq. (13) as $\mathbf{M}_f$, $\mathbf{C}_f$, $\mathbf{C}_{som}$, $\mathbf{K}_{som}$ and $\mathbf{M}_V$. The length of each of the elements is 1.0 m long in the radial direction and 0.5 m deep in the vertical direction, respectively, and the time interval is taken to be 0.1 sec.

Investigated first is the timewise variation of the water surface at the point 5 m distant from the axis of symmetry of each of models: nosp 50, nosp 10 and sponge, respectively. The volumetric drag coefficient, r, is prescribed as $r = 0.1$kN·sec/m^4.

Shown in **Fig.3**(a)~(c) are the free surface elevation when the forced heaving displacement is assigned at the frequency of $f = 0.5$Hz.

If no reflection of wave were expected, the ordinate should coincide. The results show that the waves of nosp 50 and sponge coincide very well for different time steps; however the wave of nosp 10 varies significantly showing that its surface elevation is significantly influenced by the reflection of waves. nosp 50 has not yet received the reflected waves and in sponge the wave energy seems to be well absorbed.

Considered next is the change of free surface when the length of the sponge layer and the coefficient of volumetric drag are changed. Because the volumetric drag coefficient r is an artificial parameter, its optimal value can be found only through numerical trial and error analysis. First, the sponge length is prescribed to be 20m while changing the coefficient, r, at 3 distinct levels from $r = 0.1$ to 10 kN·sec/m^4. The results are shown in **Fig.4**(a)~(c).

When $r = 10$ kN·sec/m^4, certain variation of the water elevation is observed in the fluid domain; however, no significant change of water elevation in the sponge layer can be observed. This implies the fact that for higher value of r, the resistance is so strong that the waves are reflected at the interior boundary of the sponge layer. In case the drag coefficient, r, is smaller, the reflection does not occur and the energy seems to be absorbed in the sponge layer.

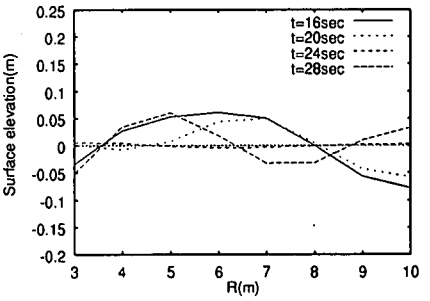

(a) nosp10 model

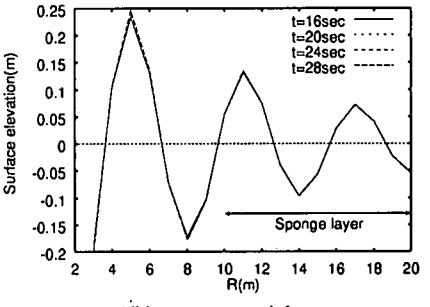

(b) sponge model

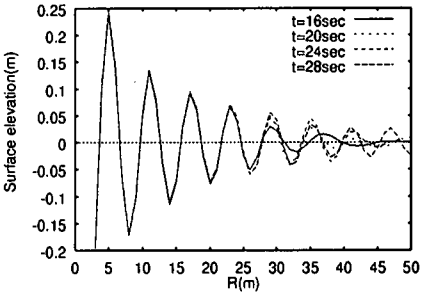

(c) nosp50 model

Fig. 3 Change of free surface elevation at $f = 0.5$Hz

Moreover, analysis is made to find the effect of the length of the sponge layer by changing it from 10 m to 20 m by keeping the distance between the central axis and the interior boundary of the sponge layer to be 10 m. Shown in **Fig.5** also are change of free surface assuming the volumetric drag coefficient, r, to be $r = 0.1$ kN·sec/m^4 and the element length in the radial direction is kept to be as small as 0.25 m.

When the length of the sponge layer is 20 m,

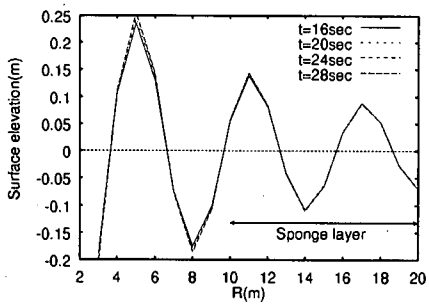

(a) r=0.1 kN sec/m^4

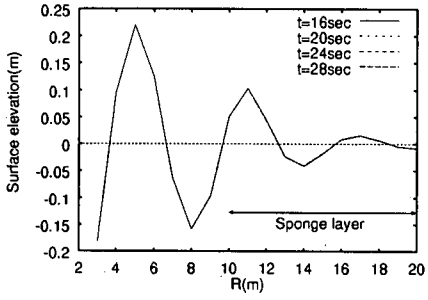

(b) r=1.0 kN sec/m^4

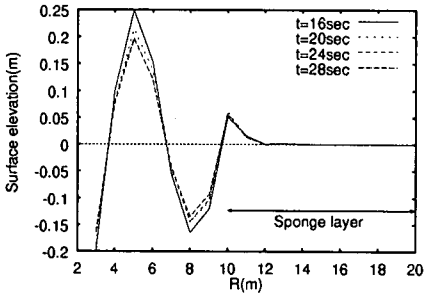

(c) r=10 kN sec/m^4

Fig. 4 Configuration of free surface for different values of resistance coefficient, r

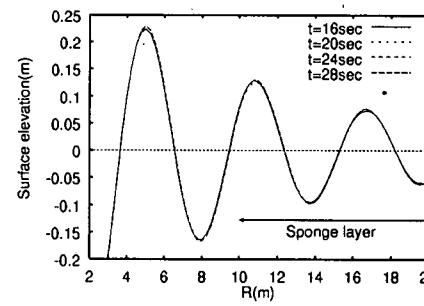

(a) length of sponge layer=10m

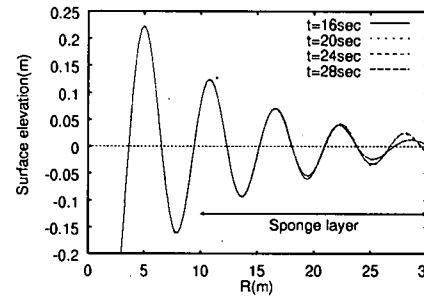

(b) length of sponge layer=20m

Fig. 5 Effect of sponge layer length on the surface elevation

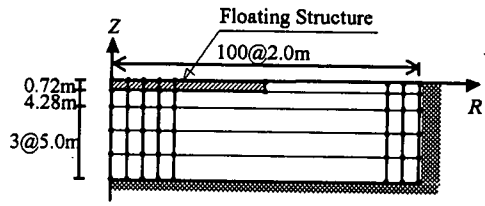

Fig. 6 Model: rigid wall at 200 m from disc

the amplitude of the response at the exterior boundary tends to be zero. From this, it may be seen that even if the volumetric drag coefficient is small, waves can be well absorbed if the length of the sponge filter is taken sufficiently long enough. In the subsequent analysis, the volumetric coefficient is set to be $r = 0.1$ kN·sec/m^4 with the length of the sponge layer to be 40m.

(2) Analysis for Airplane Landing in the Axisymmetric Problems

An attempt is made to evaluate the applicability of the sponge layer for axisymmetric airplane landing problem. Two analytical disk models of radius 200 m are considered. The first model has a rigid wall at 200 m from the boundary of the disk as shown in **Fig.6**; while the second model as shown in **Fig.7** has the sponge layer of the length 40 m at the distance 20 m from the boundary of the disk with the coefficient of volumetric drag, $r = 0.1$ kN· sec/m^4. The other characteristics remain the same as shown in **Table 1** and the time interval is taken to be 0.1 sec.

The load pattern is as shown in **Fig.8** and the maximum load is assumed to be 6615 kN including the impact force of a jumbo jet plane, and **Fig.9** shows the time history of the vertical deflection at the point of the landing. Such a loading pattern was used in the feasibility study of a floating airport [9].

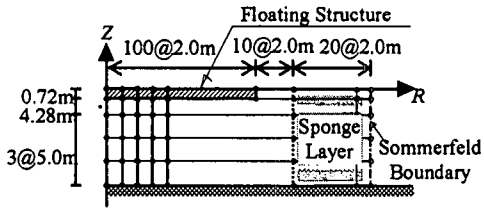

Fig. 7 Model: sponge layer at 20 m from disc

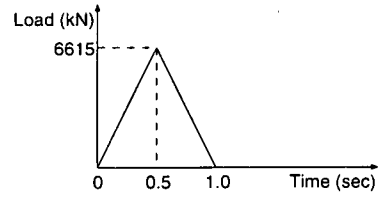

Fig. 8 Loading pattern for airplane landing

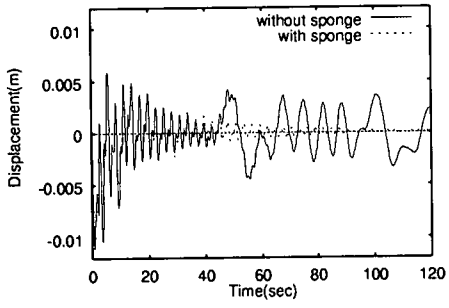

Fig. 9 Time history of vertical deflection at the point of landing

In **Fig.9**, the response obtained with sponge layer and that without sponge layer coincide very well before 20 seconds. However, it can be seen that the deflection of the model without the sponge layer becomes significantly large after 45 seconds from the landing. This implies that once propagated wave is reflected at the rigid wall located at 200 m away from the boundary of the disk and comes back to the center about 45 seconds later. On the other hand, in the model with the sponge layer the displacement is damped out gradually to become zero finally. From these results, it can be seen that even for irregular waves, the wave energy can be absorbed very well by the sponge layer. It should also be pointed out that the generated waves are irregular and have wide frequency range, thus it is obvious that sole application of Sommerfeld boundary without sponge

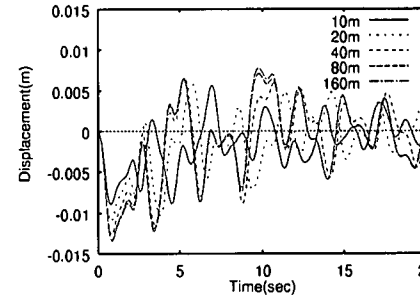

Fig. 10 Effect of depth of water upon vertical deflection at the point of landing

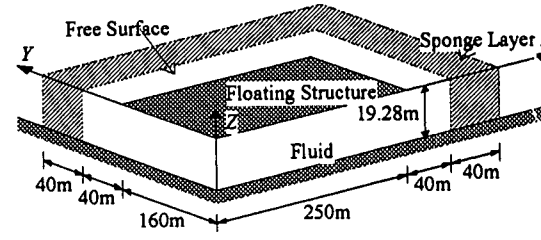

Fig. 11 Model for 3-dimensional analysis (Model 1)

layer as an open boundary fails for the absorption of wave energy for a wide frequency range.

Next, the effect of the depth of fluid is studied on the model as shown in **Fig.7** while keeping the other parameters remain unchanged. The depth is varied to be 10 m, 20 m, 40 m, 80 m and 160 m. **Fig.10** shows the time history of the vertical displacement of the loaded point.

It can be seen that the time for the maximum response depends on the depth of fluid and the first peak value of the vertical displacement increases as the water depth increases. However, if two cases of depth 80m and 160 m are compared, they seem to give the similar results. Thus, it may be apparent that when the depth is large enough, no significant difference can be observed in the response. Investigation of the pressure distribution along the vertical axis through the point of landing has shown that as the water depth decreases the pressure on the sea bottom as well as that on the bottom surface of the structure increases. This will be the reason why the response decreases as the water depth decreases.

(3) Analysis of 3-dimensional Problem

Fig.11 shows a 3-dimensional model analyzed. The size of the floating structure is 500 m × 320

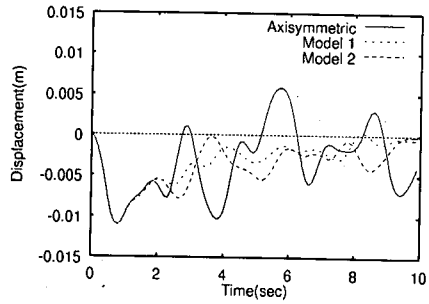

Fig. 12 Comparison of time history of vertical displacement at the point of landing

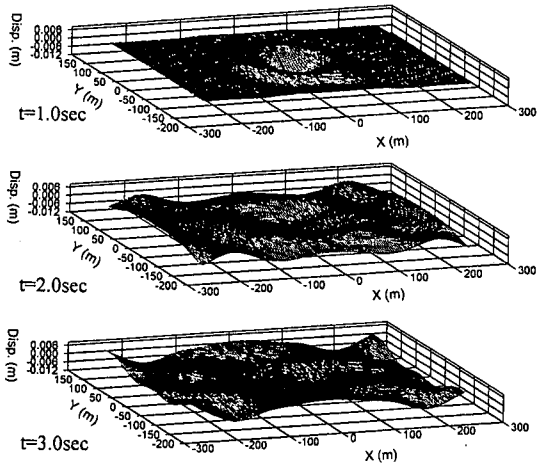

Fig. 13 Deflectional configurations (Model 1)

m (Model 1). The landing load is applied at the center of the structure, and thus the analysis can be made assuming double symmetry about x- and y-axis. The load pattern is as shown in **Fig.8**.

For the floating structure, 8-node elements with second order polynomial are used; whereas, for the fluid and sponge layer, 20-node elements with second order polynomial are used with only a single layer in the vertical direction. Even in such an analysis, the D.O.F. amounts to about 70 thousands, which is the reason why the size of 500 m × 320 m has been chosen as the model of a floating runway.

For comparison, Model 2 with the size of 320 m × 320 m has also been analyzed. Shown in **Fig.12** are the vertical displacements at the loaded point. Also shown in **Fig.13** and **Fig.14** are the time variation of the shape of deflection for Models 1 and 2, respectively.

It can be seen that up to 2 sec, the axisymmetric deformation is conspicuous; after 2 sec, however, the effect of the rectangular edge of

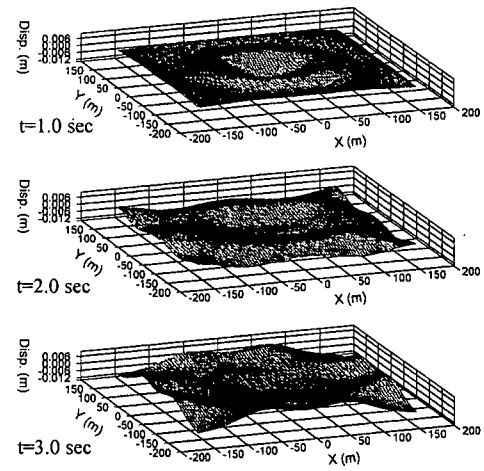

Fig. 14 Deflectional configurations (Model 2)

the floating structure becomes significant reflecting the basic characteristic vibration mode of the floating structures. This will explain why the displacement responses are different to each other after 2 sec. It must be born in mind, however, that for the response analysis immediately after the landing, the symmetric model will be thought to be sufficient for practical purposes to find the maximum response.

(4) Analysis of Moving Load

So far, consideration has been limited to the triangular loading pattern as shown in **Fig.8**. Herein, the load will be slided to see the effect of the landing of airplane in more practical manner and the Model 1 is used for the floating airport. It is assumed that although it is necessary to consider the braking and the slowing down, the plane maintains the speed of 50 m/sec after the landing. Also, the first landing takes place at the point 60 m from the edge of the floating airport. After the landing, the load has less impact so that the maximum load is only 3920 kN and the load pattern is of the similar triangle with the load duration of 0.8 sec. The sequence of loadings are applied at points at every 20 m after the landing along the runway. They are applied at the two nearest adjacent nodal points from the loading point as concentrated forces, of which magnitudes are determined in proportional to the distances from the nodal points of the opposite side to the loading point.

Using this procedure, the evaluation of the response of PAPI is studied. The location of PAPI is 50 m away from x-axis from the point of landing. Thus, the location of PAPI is (-190 m, 50 m, 0) in the coordinate system shown in **Fig.11**,

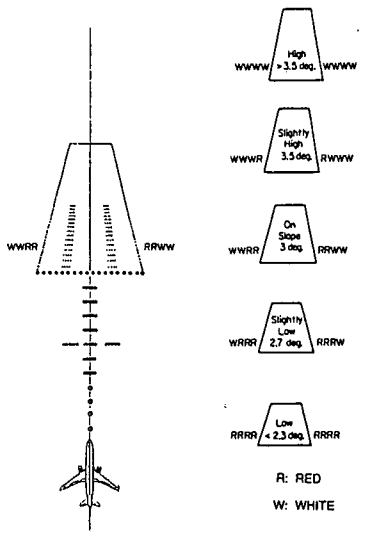

(a) general view

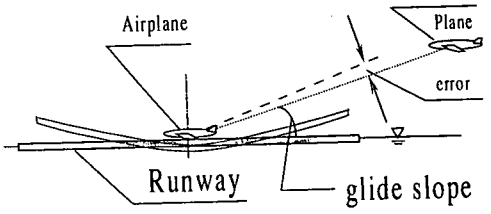

(b) occurance of error angle

Fig. 15 PAPI, Precision Approach Path Indicator

and the angle of slope at this point is to be investigated as shown in **Fig.15**[2].

Fig.16 shows the angles of rotation about x- and y-directions where the allowance limit for the error, 1'(= 0.017°) is indicated.

Although the error angle about x-axis is larger, it does not exceed the allowance limit. It can be therefore concluded that as for the floating structure considered herein, the PAPI can be thought to fulfill its function within a good accuracy.

Finally, the scenario of the deflection of the rectangular airport is shown in **Fig.17** up to 4 sec after the landing. The maximum deflection of the deck is about 1.6 cm, which seems to be small enough.

In this paper, results on the sectional forces are not indicated; however once the vertical displacement of a thin plate is obtained the calculation of the sectional forces are straightforward, and our

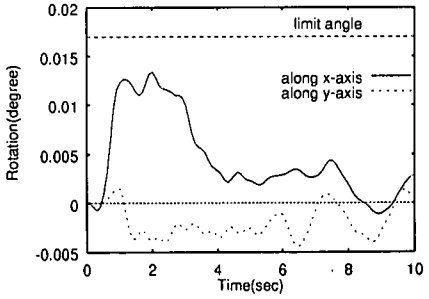

Fig. 16 Angle of rotation and allowance limit

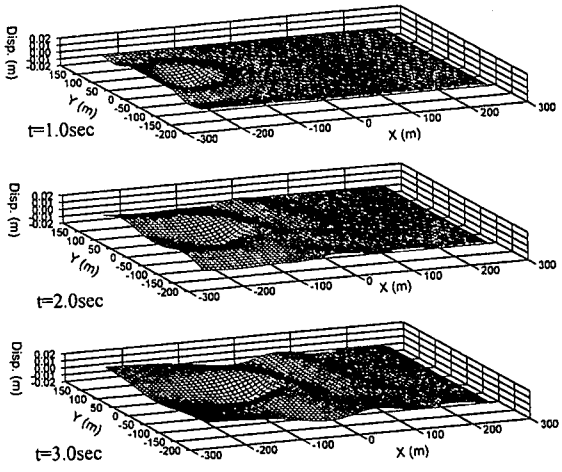

Fig. 17 Deflections due to moving aircraft

main concern is to examine the effect of airplane landing on PAPI rotation, so they are omitted in this paper.

4. CONCLUDING REMARKS

The following concluding remarks will be made:

1. The sponge layer is found to be very effective to dissipate the wave energy and is particularly suited for the conversion from a closed finite domain to the domain with the open boundary. It must be kept in mind, however, that the volumetric drag coefficient must be kept not too large so that the reflection of waves will not occur at the boundary of the sponge, and the length of the sponge should be taken sufficiently long.
2. When a floating structure is loaded with the landing airplane, the response of the floating structure will be affected by the distance between the bottom of the structure and the seabed. Nevertheless, when the depth is suf-

ficiently large, its effect becomes very small.
3. When a large rectangular floating structure is loaded with the impulsive landing load, a deflectional shape of concentric circular indentation occurs for the initial few seconds in such a way that the deflection can be predicted using an axisymmetric model; however, after such a few second, the response depends on the natural vibrational mode of the structure.
4. The maximum displacement response of the floating airport occurs within a few seconds after landing. Thus, for practical purposes of finding only the maximum displacement, the floating airport can be thought to be modeled as an axisymmetric disk model can be used. However, if the response analysis is required for a long period of time, then more exact modeling is required.

REFERENCES

1) Wu, C., Utsunomiya, T. and Watanabe, E.: Harmonic wave response analysis of elastic floating plates by modal superposition method, *Structural Eng./Earthquake Eng., JSCE*, Vol.14, No.1, pp.1s-10s, 1997.
2) Yamamoto, H.: Concept for a super-large floating structure, *Proc. International Workshop on Floating Structures in Coastal Zone*, Hiroshima, Port and Harbour Research Institute, Ministry of Transport, pp.121-136, 1994.
3) Watanabe, E. and Utsunomiya, T.: Transient response analysis of a VLFS at airplane landing, *Proc. International Workshop on Very Large Floating Structures*, Hayama, Ship Research Institute, Ministry of Transport, pp.243-247, 1996.
4) Watanabe, E., Utsunomiya, T. and Taenaka, S.: Transient hydroelastic analysis of a very large floating structure by finite element method, *J. of Structural Engineering*, JSCE, Vol.43A, pp.49-54, 1997 (in Japanese).
5) Ohyama, T. and Nadaoka, K.: Development of a numerical wave tank in nonlinear and irregular wave field with non-reflecting boundaries, *Proceedings of JSCE*, No.429/II-15, pp.77-86, 1991 (in Japanese).
6) MacNeal, R.H.: *NASTRAN Theoretical Manual*, The MacNeal-Schwendler Corporation, 1969.
7) Hibbitt, Karlsson and Sorensen, Inc.: *ABAQUS Users Manual*, ver.5.5, 1995.
8) Hibbitt, Karlsson and Sorensen, Inc.: *ABAQUS Theoretical Manual*, ver.5.5, 1995.
9) Takarada, N.: An example of technology assessment of VLFS (Part 5), *Proceedings of SNAJ*, No.642, pp.702-719, 1982 (in Japanese).

(Received July 14, 1997)

有限要素法による大規模浮体構造物の過渡応答解析

渡邊英一・宇都宮智昭・谷垣信吉

本研究は, 航空機着陸荷重による超大型浮体式構造物の過渡応答解析を有限要素法により行ったものである. 不規則波に対して開境界条件を適用するため, スポンジ層と Sommerfeld 境界を組み合わせた波浪吸収フィルターを適用し, その有効性を確認した. また, 航空機着陸を模擬した荷重による浮体の応答特性は, 着陸から数秒間は軸対称形状となるが, それ以後は浮体の形状の影響を大きく受け, 非軸対称形状となる事を示した.